Journal of Controlled Release 305 (2019) 120–129

Contents lists available at ScienceDirect

Journal of Controlled Release

journal homepage: www.elsevier.com/locate/jconrel

NIR-responsive ROS generating core and ROS-triggered 5′-Deoxy-5-fluorocytidine releasing shell structured water-swelling microgel for locoregional combination cancer therapy

Junghan Lee, Ratchapol Jenjob, Enkhzaya Davaa, Su-Geun Yang*

Department of New Drug Development, Inha University College of Medicine, B-308, Chungsuk Bldg., 366, Seohae-Daero, Jung-Gu, Incheon 22332, Republic of Korea.

ARTICLE INFO

Keywords:
Combination cancer therapy
Photodynamic therapy
Swelling microgel
Pheophorbide A
Triggered drug release
Poly(2-hydroxyethyl methacrylate)
Chitosan

ABSTRACT

Combination chemotherapy now becomes the most standard cancer treatment protocol. Here, we present a core-shell type polymeric microgel (CSPM) which combines photodynamic and chemo therapeutic modalities in one-pot system. CSPM localizes in the malignant lesion after intratumoral injection, releases reactive oxygen species (ROS) and anticancer drug (5′-deoxy-5-fluorocytidine; DFCR) under the near-infrared (NIR) laser treatment. Pheophorbide A (PheoA)-linked poly(hydroxyethyl methacrylate) (poly-HEMA) was designated to a ROS-generating core, and chemically covered with a chitosan shell. In addition, phenylboronic acid was employed in chitosan shells and linked to DFCR to form an ROS cleavable boronic ester. The core-shell structure of CSPM was determined by transmission electron microscopy. NIR-responsive photodynamic ROS generation was confirmed by the oxidative reduction of 9,10-dimethylanthracene (a fluorescent dye), and the cascadic release of DFCR by ROS was confirmed by a release study and a live and dead cell imaging study. Typically, poly-HEMA cored microgel increased its volume by 48.9-fold after absorption of body fluid. This swelling property ensured CSPM was retained in tumor tissues after subtumoral injection and the suitability of CSPM for locoregional phototherapy. The therapeutic effect of CSPM was attributed to the combined, cascadic deliveries of cytotoxic ROS and DFCR and confirmed by growth inhibition studies in in vitro pancreatic cancer cells and in vivo colon cancer mouse model.

1. Introduction

The development of small molecule anticancer drugs has revolutionized the past decade through the increased understanding of tumor biology and genetics. Molecular targeting drugs have been precisely designed, optimized and able to inhibit oncoproteins at nanomolar concentration [1–3]. However, the efficacy of these drugs is still under question. Shutdown of a single pathway is not sufficient to induce full remission of the cancer because of cancer genetic heterogeneity and bypassing cellular signals. On the other hand, clinical scientists have begun to realize combination chemotherapy, which targets multiple cancer signals, is more potent, effective, and less toxic than monotherapy in terms of patient survival and start to investigate the combination regimens of these molecular targeting drugs [4–6].

Photodynamic therapy (PDT) can be designed as the best therapeutic component for the combination cancer therapy [7]. Furthermore, locoregional treatment therapy which can dramatically reduce the systemic side effects can be achieved through the PDT [8]. Reactive oxygen species (ROS) generated by photosensitizers are the major therapeutic modality of PDT. Photosensitizers are usually introduced via systemic injection. Interestingly, photosensitizers selectively accumulate more in tumor tissues than normal tissues. The accumulation amount of photosensitizers in tumor tissues is two or three times larger than that of normal tissues. PDT is performed via subsequent locoregional irradiation of tumor tissue with a near-infrared (NIR) laser. Many clinical data have demonstrated PDT is one of the best options for combinational chemotherapy [9]. Ortner et al. reported the efficacy of combination therapies (PDT plus conventional stent treatment in 20 patients with unresectable cholangiocarcinoma). Notably, this clinical study was terminated earlier than scheduled because survival benefit was significantly higher in the combination treatment group than in the conventional group [10]. Many other studies also proved the beneficial effects of the combination PDT therapy with anticancer drugs [11–18].

Photodynamic ROS can be applied not only to cancer therapy, but also to stimuli-responsive drug delivery systems. Scientists have studied cancer cell-specific ROS responsive drug delivery system for decades.

* Corresponding author.
E-mail address: sugeun.yang@inha.ac.kr (S.-G. Yang).

https://doi.org/10.1016/j.jconrel.2019.05.016
Received 5 January 2019; Received in revised form 1 May 2019; Accepted 12 May 2019
Available online 13 May 2019

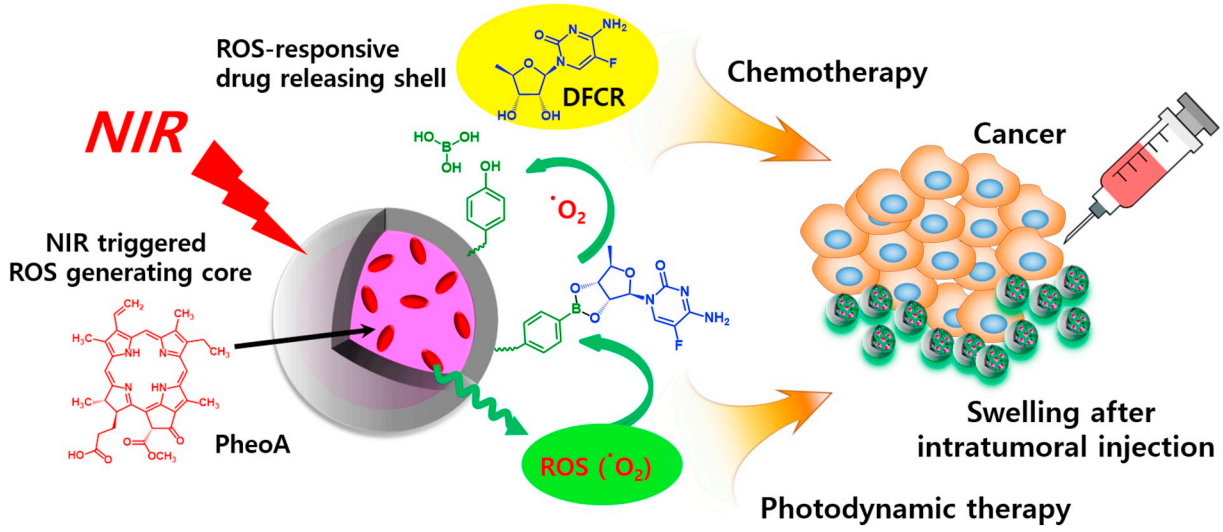

Scheme 1. Core-shell type (CSPM-PheoA-DFCR) microgels for photodynamic, chemo and locoregional combination chemo therapy. NIR (670 nm) irradiation generates cytotoxic ROS from photodynamic agent (Pheophorbide A; PheoA) in core system. And then the ROS triggers the release of DFCR which is conjugated on to chitosan shell via ROS-cleavable linker.

Various ROS-cleavable linkers, such as thioethers, selenium, thioketal, aminoacrylates, boronic acid esters, peroxalate esters, and polyproline, have been developed to achieve ROS-responsive cancer targeting [19–21]. Generally, cancer cells contains higher concentration of ROS than normal cells, and linkers have been designed to be cleaved in response to cancer cell-specific ROS and released the linked drug. However, cancer cell-specific ROS is not always enough to trigger cancer cell-specific drug release. ROS scavenging power of cancer cells is much higher than that of normal cells and ROS is effectively scavenged under the toxic concentration for the cell survival. On the contrary, normal cells sometimes show much high ROS concentration under certain conditions such as infection, diabetic mellites and etc. [22–24]. Therefore, locoregional PDT, which can dramatically increase local ROS concentrations, may offers an attractive way to achieve ROS-responsive and cancer-specific drug release.

In this study, we designed a core-shell type polymeric microgel containing an ROS-generating photosensitizer (Pheophorbide A; PheoA) in core system and an ROS-cleavable drug (5′-deoxy-5-fluorocytidine; DFCR) in the shell (CSPM-PheoA-DFCR, see Scheme 1). PheoA-core microgel particles (CSPM-PheoA) were produced polymerizing HEMA monomers in the presence of chitosan [25,26]. Phenylboronic acid (PBA; a linker molecule) was introduced to chitosan shells and coordinated with DFCR to form CSPM-PheoA-DFCR. PBA forms a cyclic boronic ester with DFCR (a diol) that acts as ROS-cleavable linker [27]. According to our hypothesis, ROS, such as $^{-}O_2$, O^{2-}, $O_2{}^{2-}$, H_2O_2, are generated, when PheoA located in microgel is activated by near-infrared (NIR) light. Singlet oxygen and oxygen radicals ($^{-}O_2$, O^{2-}, and $O_2{}^{2-}$) are toxic to cells and the H_2O_2 generated breaks the ester linkage between PBA and DFCR and triggers DFCR release. To investigate this hypothesis, we synthesized and characterized core/shell microgel particles and evaluated their photo-induced therapeutic effects on human pancreatic cancer (PANC-1) cells and in a murine colon cancer (CT-26) model.

2. Materials and methods

2.1. Materials

Chitosan (Mw 50,000–190,000, > 75% deacetylation), HEMA (2-hydroxyethyl methacrylate), TBHP (*tert*-butyl hydroperoxide), EDC (1-ethyl-3-(3-dimethylaminopropyl) carbodiimide), PBA (4-(hydroxymethyl)phenylboronic acid), CDI (carbonyldiimidazole), and DMAP (4-(dimethylamino)pyridine) were purchased from Sigma-Aldrich (St. Louis, MO). DFCR (5′-deoxy-5-fluorocytidine) was purchased from Ark Pharm (Arlington Heights, IL) and PheoA (Pheophorbide A) was obtained from Frontier Scientific, Inc. (Logan, UT). All other chemical solvents were of HPLC grade and purchased from Ducksan Chemicals Co. Ltd. (Ansan-si, Gyeonggi-do, Korea).

2.2. Syntheses of CSPM and CSPM-PheoA microgel particles

CSPMs were prepared using a previously reported method with a slight modification [28]. Briefly, 50 ml of chitosan solution (5 mg/ml) in distilled water containing 1 wt% acetic acid was added to a 100 ml 3-neck round bottom flask and vigorously stirred at 80 °C under N_2 for 30 min. HEMA monomer (1 ml) and TBHP aqueous solution (1 ml; 5 mM) were then injected into the flask. The polymerization reaction (initiated by TBHB addition) was allowed to continue for 2 h, and the synthesized CSPM microgel was then purified by dialysis (MWCO 15 K, Spectrum Lab, Rancho Dominguz, CA) for 2 days and freeze-dried.

To synthesize CSPM-PheoA, HEMA-PheoA monomer conjugates were prepared beforehand using a method similar to one previously reported [29]. Briefly, PheoA (50 mg, 84.4 μmol) was dissolved in methanol (10 ml) and then EDC (51 mg, 270 μmol) and DMAP (33 mg, 270 μmol) were added with vigorous stirring at room temperature. HEMA monomer (1.4 mmol) was then added and allowed to react in the dark with stirring for 24 h. After vacuum drying, PheoA conjugated HEMA monomers were washed with distilled water several times, collected by centrifugation, and freeze-dried.

As-prepared HEMA-PheoA monomer was further reacted with chitosan to synthesize CSPM-PheoA. HEMA (1 ml) and HEMA-PheoA conjugate monomer mixture (1:0.05 mol ratio) were added to 250 mg of chitosan containing solution in the presence of TBHP under N_2 at 80 °C for 2 h. The synthesized CSPM-PheoA was further purified by dialysis and freeze-dried.

2.3. Preparation of CSPM-PheoA-DFCR microgel

First, DFCR was complexed with phenylboronic acid to form ROS-cleavable phenylboronic ester. Briefly, DFCR (735 mg, 3 mmol) was mixed and reacted with PBA (452 mg, 3 mmol) in anhydrous DMSO 100 ml overnight. The PBA/DFCR complex so prepared was directly conjugated to CSPM-PheoA microgel without further purification. To synthesize CSPM-PheoA-DFCR complex, 8 mg of dried CSPM-PheoA

was dissolved in anhydrous DMSO (20 ml) containing CDI (73 mg, 450 μmol) and then 10 ml of PBA/DFCR (30 mM in anhydrous DMSO) was slowly added. After overnight reaction in the dark place, the conjugate mixture was further purified by dialysis (MWCO 15 k) against DMSO dialysate.

2.4. Estimation of NIR-triggered ROS generation

To detect singlet oxygen generation from CSPM-PheoA by NIR-irradiation, we used the fluorescence probe DMA (9, 10-dimethylanthracene), as previously described [30]. DMA (final conc. 100 μM) was added to CSPM-PheoA (4.5 mg/ml) in DMSO, and directly exposed to an NIR laser (λ = 671 nm, 167 mW/cm^2, Shanghai Laser & Optics Century Co., Ltd., China). The fluorescence intensities (at λ_{max} = 420 nm) of DMA were measured after different irradiation times (t = 0, 1, 2, 3, 4, 5, 10, and 30 min) using a microplate reader (Infinite 200 pro, Tecan, Männedorf, Switzerland).

2.5. Estimation of ROS-triggered DFCR release

The release profile of DFCR from CSPM-PheoA-DFCR by ROS was investigated by HPLC. Briefly, microgel samples (5 mg/ml) were exposed to NIR (λ = 671 nm, 167 mW/cm^2, Shanghai Laser & Optics Century) for different times (0, 1, 2, 3, 4, 5,10, and 30 min) and precipitated by centrifugation at 13,000 rpm for 30 min. DFCR of supernatant were then subjected to HPLC (Alliance 2695 equipped with a 2487 detector; Waters, MA, USA) using the following conditions; column size 4.6 × 160 mm, particle size with 5 μm (GL Sciences, Japan), injection volume = 10 μL, elution buffer DW/methanol (8:2, *v/v*), absorbance λ = 220 nm.

2.6. Cell culture

PANC-1 (a human pancreatic carcinoma cell line) and CT-26 (murine colon carcinoma) cell lines were grown in DMEM (Dulbecco's modified Eagle's medium) containing 10% FBS (fetal bovine serum), 1% penicillin, and 1% streptomycin.

2.7. Estimation of cellular cytotoxicity

A WST (water-soluble tetrazolium) assay was used to investigate the cellular toxicity of microgels. Cells (4 × 10^4 per well) were seeded on a 94-well plate and incubated for 24 h in a 5% CO_2 incubator at 37 °C, and then DFCR, CSPM or CSPM-PheoA were added at different concentrations. After incubation for 24, 48, or 72 h, WST-1 was added to each well and incubated for 4 h according to the manufacturer's instructions. Cell viabilities were analyzed by measuring absorbance (450 nm) using a microplate reader (Infinite 200 pro, Tecan, Männedorf, Switzerland). To evaluate the PDT effect, cells in 5% DMSO medium were treated with CSPM-PheoA or CSPM-PheoA-DFCR in DMSO (final conc. 65 μg/ml) and the exposed to a NIR laser (λ = 671 nm, 100 J/cm^2) for 2 h, after which cell viability testing was using WST-1 as described above. The results of 5 independent sample sets were averaged.

2.8. Cell imaging

The cytotoxic effects of NIR triggered ROS release from microgels were investigated by cell imaging. PANC-1 cells (50,000 cells/well) were seeded in glass-bottomed 8-well chamber slides (Lab-Tek) in 0.5 mL DMEM and incubated for 24 h at 37 °C in a 5% CO_2 atmosphere. The same amounts of CSPM, CSPM-PheoA, or CSPM-PheoA-DFCR microgel in DMSO (25 μL, 4.6 mg/ml) were then added and cells were incubated for 2 h. Cells were then exposed to NIR for 10 min and incubated for another 2 h. They were then stained with nuclear staining dyes (ReadyProbes cell viability imaging kit, Blue/Green, Thermo Fisher) according to the manufacturer's instructions, and washed with fresh PBS buffer 3 times. After 4% paraformaldehyde fixation, cell images were obtained using a confocal microscope (FV1000, Olympus).

2.9. In vivo tumor growth inhibition study

BALB/c mice (Orient-Bio, Gyeonggi-do, Korea) weighing 15–20 g were housed in conventional cages with free access to water and rodent chow at 25 °C with a 12 h dark/light cycle. All procedures involving laboratory animal use were in accordance with the guidelines for animal experiments established by the IACUC INHA-University. All animals received humane care with unlimited access to chow and water.

Murine colon carcinoma CT-26 cells (2.5 × 10^6) were subcutaneously injected into both sides (left and right) and into the backs of BALB/c mice. When primary tumors reached ~100 mm^3 in size, mice were divided into four groups (n = 3) and three microgels (CSPM, CSPM-PheoA, or CSPM-PheoA-DFCR) or PBS (without microgel) were directly injected into tumors at a dose of 10 mg/kg. Each left side tumor was then irradiated with a NIR laser (λ = 671 nm, 100 J/cm^2) once a day for 3 days. Primary tumor sizes (maximum dimension determined using a vernier caliper) and body weights were recorded daily, and all mice were sacrificed 2 weeks after injections. Excised tumors were analyzed by H&E (hematoxylin and eosin) staining and using a TUNEL (terminal deoxynucleotidyl transferase dUTP nick end labeling) assay.

3. Results and discussion

3.1. Synthesis of core and shell forming monomers and polymeric microgel

CSPM-PheoA and CSPM-PheoA-DFCR particles were successfully synthesized as shown in Fig. 1. To produce CSPM, HEMA was used as a core-forming and crosslinking material, as described previously [28]. Schematic illustration of CSPM core-shell forming mechanism was described in SI Fig. S1. The carboxyl group of PheoA directly reacted with the hydroxyl group of HEMA monomer to form an ester bond in the presence of N-(3-dimethylaminopropyl)-N′-ethylcarbodiimide (EDC) and 4-dimethylaminopyridine (DMAP) (Fig. 1A). HEMA-PheoA was analyzed by Fourier transform infrared spectroscopy (FT-IR), and specific peaks were observed at 1735.8 cm^{-1} (C═O stretch) and 1153.9 cm^{-1} (C—O—C bend) (SI Fig. S2). Microgel particles were produced by adding HEMA monomers and HEMA-PheoA conjugate mixture (HEMA 1 g, HEMA-PheoA 16 mg, HEMA: HEMA-PheoA = 1: 0.002 M ratio) to chitosan solution (250 mg) in the presence of tert-butyl hydroperoxide (TBHP; initiator). The CSPM-PheoA produced was purified by dialysis (molecular weight cut-off 15 kDa). PheoA content was determined to be 0.14 wt% by UV–Vis spectrometry (conjugation efficiency; ~11%, initial reaction amount of HEMA-PheoA 1.25 wt% of chitosan, HEMA, and HEMA-PheoA reaction) using a standard free PheoA concentration versus absorbance plot (SI Fig. S3). PBA-DFCR was then conjugated to CSPM-PheoA (Fig. 1B, C). Briefly, 4-(hydroxymethyl) phenylboronic acid and DFCR (1:1 M ratio) were allowed to react for 24 h in anhydrous dimethyl sulfoxide (DMSO), and then mixed with CSPM-PheoA in the presence of CDI to produce the ester by reaction between the amine moiety of chitosan and hydroxyl group of PBA-DFCR. After purifying the CSPM-PheoA-DFCR produced by dialysis, it was subjected to ^{1}H NMR. As shown in SI Fig. S4, chitosan polymer (Fig. S3A) alone produced a specific peak at 2 ppm (3H (1), attributed to the acetyl group). CSPM-PheoA (SI Fig. S4B) showed characteristic peaks at 2.4 ppm (3H (2), in PheoA), 1.1 ppm (3H (3), in PheoA), and small multiplet at 1.4–1.9 ppm (3H (4, 5), which was attributed to the methyl groups of PheoA conjugated HEMA backbone. CSPM-PheoA-DFCR (SI Fig. S4C) showed specific peaks at 8.1 ppm (H (6), NH group of the carbamate bond), 5.1 ppm (2H (7), methyl group of PBA), 7.7 ppm (H (8), aromatic ring of PBA), and 7.5 ppm (H (9), in its DFCR moiety). The amount of conjugated DFCR in CSPM-PheoA-DFCR was analyzed by integrating peaks at 1.1 ppm (3H (3), PheoA)

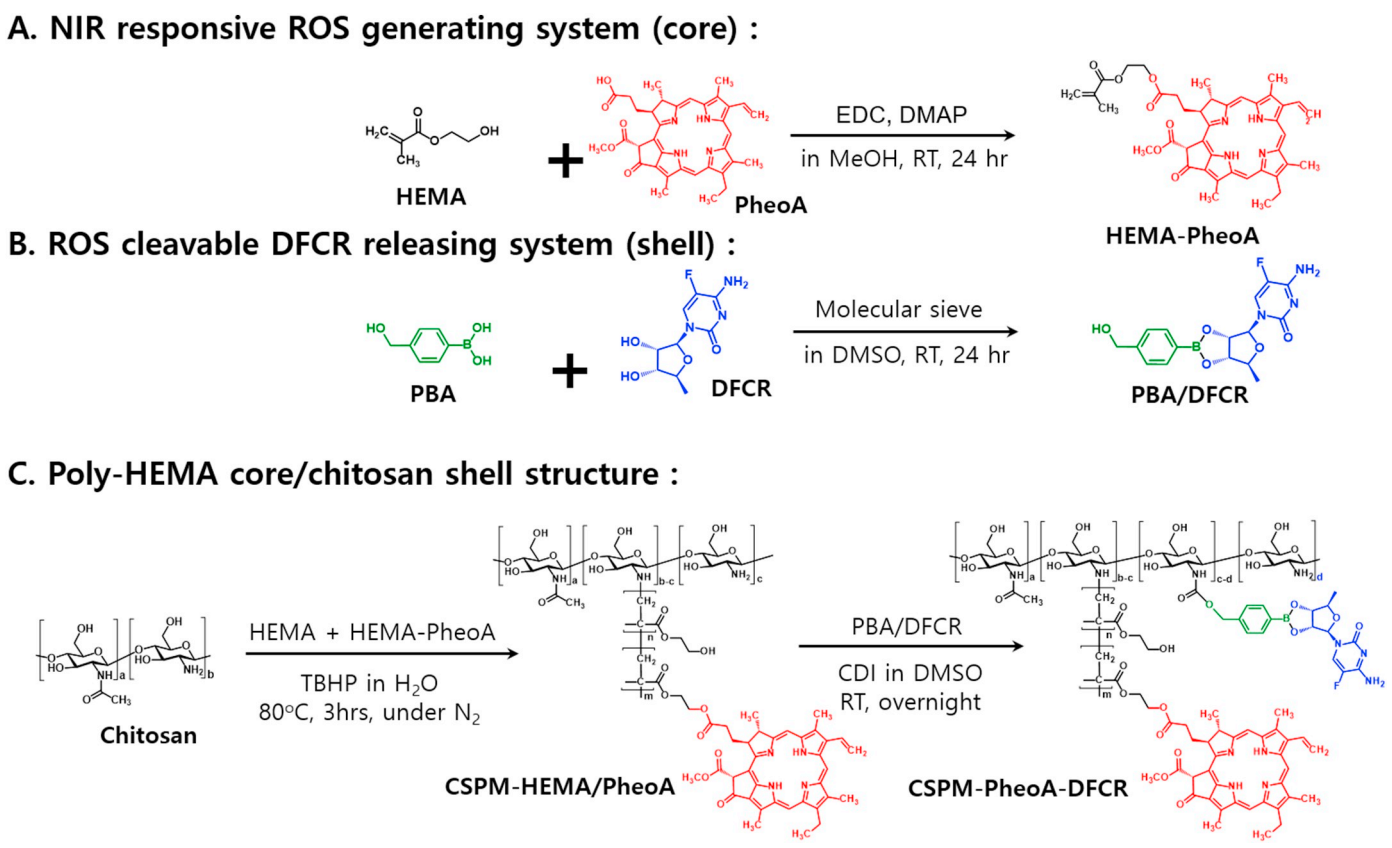

Fig. 1. Synthesis of (A) HEMA-PheoA conjugate, (B) PBA/DFCR complex, and (C) CSPM-PheoA-DFCR microgel; HEMA: (hydroxyethyl)methacrylate, CSPM: poly-HEMA/chitosan microgel particle, PheoA: pheophorbide A, PBA: 4-(hydroxymethyl)phenylboronic acid, DFCR: 5′-deoxy-5-fluorocytidine, TBHP: *tert*-butyl hydroperoxide, CDI: carbonyldiimidazole, EDC: N-(3-dimethylaminopropyl)-N′-ethylcarbodiimide, DMAP:4-dimethylaminopyridine, MeOH: methanol, and DMSO: dimethyl sulfoxide.

and 8.1 ppm (H (6), the carbamate NH group) in the ^{1}H NMR spectrum, and calculated to be around 33 mol% of PheoA in the CSPM-PheoA microgel.

3.2. Core-shell structure of CSPM-PheoA-DFCR microgel

The synthesized CSPM-PheoA-DFCR microgel was dispersed in water and its absorption/emission spectra and particle size distribution were measured by UV–vis spectrometer, fluorimeter, dynamic light scattering (DLS) and transmission electron microscopy (TEM). CSPM in water (Fig. 2A) showed a broad absorption band induced by the CSPM microgel, whereas CSPM-PheoA particles (Fig. 2B) produced a strong fluorescence signal in the 600–800 nm range and specific absorption peaks attributable to PheoA in the CSPM microgel. TEM images of CSPM clearly showed core-shell structure of microparticles (Fig. 2C). To understand particle structures in more detail, CSPM particles were analyzed by TEM and we further conjugated a green fluorescent dye, namely, NHS activated Oregon green, to the amine residues of chitosan in CSPM-PheoA particles, and then examined them under a fluorescence microscope. Fluorescence microscopic images (Fig. 2D) showed that approximately 1 μm sized particles exhibited Oregon green and red PheoA fluorescence in the same parts of particles, indicating HEMA-PheoA monomers and HEMA were properly conjugated to chitosan during microparticle preparation and formed core-shell structure.

3.3. Colloidal stability of CSPM microgel

To measure the colloidal stability of CSPM, we monitored time dependent hydrodynamic sizes of CSPM in water, PBS, and 10% FBS containing DMEM medium by DLS (Dynamic light scattering) analysis. And the morphology of particles incubated for 24 h was further confirmed by TEM (transmission electron microscopy) (SI Fig. S5). As shown in Fig. S5A, there was no change in hydrodynamic size of CSPMs in water and PBS, but the particle size in DMEM medium increased over time. TEM images clearly show the particle stability in different medium condition (Fig. S5B). CSPM in water showed highly monodispersed with spherical shapes. In PBS, phosphate salts were absorbed on the particle surface which were observed in low magnification TEM images (only dry state). But no aggregation or precipitation of microgels were observed in PBS buffer (wet state). In the case of DMEM, CSPM particles showed time-dependent aggregation due to the interaction between CSPM and various proteins in the medium. Based on our design, CSPM will be stored in dry state and reconstituted using PBS for an injection. So, we believe 1 or 2 h of stability in PBS buffer will be enough for an injection. Furthermore, CSPM and CSPM-PheoA microgels (SI Figure S6A1 and A2) in water produced stable turbid colloidal suspensions without aggregation and CSPM-PheoA exhibited red fluorescence when exposed to UV light (wavelength = 365 nm) (SI Figure S6B2). These water absorption and swelling characteristics suggest CSPM microgel can be injected directly into tumors and facilitate localized PDT-induced drug release.

3.4. Swelling properties of CSPM-PheoA-DFCR microgel

The mean hydrodynamic size of CSPM particles as determined by DLS was 1309 ± 306 nm, and their mean dry diameter by TEM was 511 ± 59 nm (Fig. 3A). Mean hydrodynamic particles sizes of CSPM-PheoA were 1214 ± 320 nm (DLS) and 332 ± 30 nm (TEM) (Fig. 3B), and these were unchanged by conjugation between CSPM-PheoA and DFCR. These results showed particle sizes appeared to be highly

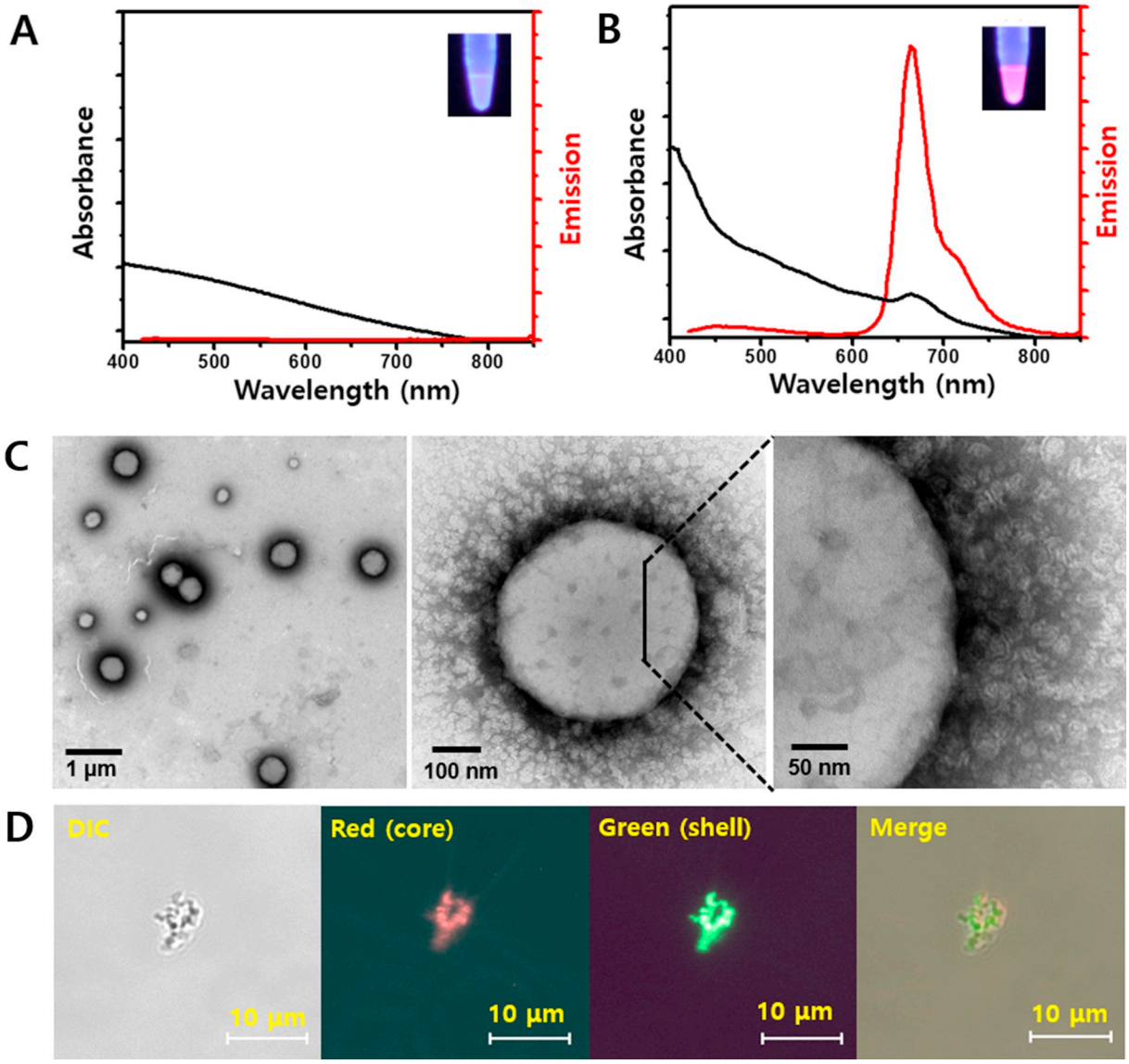

Fig. 2. Core-shell structure of CSPM-PheoA-DFCR microgels. Absorption/Emission spectra of CSPM microgels (A) and CSPM-PheoA microgels (B) (inserted images: fluorescence of samples under UV 360 nm). PheoA, located in core structure of microgel, shows specific absorption and emission peaks. (C) TEM images of CSPM-PheoA-DFCR microgels, showing the black-stained chitosan shell in ~ 50 nm thickness and poly-HEMA core. (D) Fluorescence microscopic observation of CSPM-PheoA-DFCR microgels. Oregon green conjugated with amine of chitosan shell emits green fluorescence, and PheoA conjugated with poly-HEMA core emits red fluorescence. (For interpretation of the references to colour in this figure legend, the reader is referred to the web version of this article.)

dependent on water content, and thus, volume swelling ratios were calculated using the following equation: [31,32].

$$\text{Volume swelling ratio} = \frac{\text{V wet}}{\text{V dry}} = \frac{\text{rwet3}}{\text{rdry3}}$$

V_{wet}: wet sample volume, V_{dry}: dry sample volume, r_{wet}: wet particle radius as determined by DLS, r_{dry}: dried particle radius as determined by TEM.

As observed in Fig. 3C, the volume swelling ratio of CSPM-PheoA is found to be much larger than that of CSPM (48.9 vs. 16.8). In addition, we observed that the particle size of CSPM-PheoA was much smaller than that of CSPM, presumably because of the hydrophobic nature of PheoA.

Therapeutic efficacy of locoregional cancer therapy using drug eluting hydrogels appears to be strongly influenced by the physical properties of the hydrogel itself. Generally, swelling of microgel after locoregional injection facilitate the drug release and dramatically enhances the local drug concentration [33]. Recently, Zhang et al., reported light-induced swelling cellulose hydrogel which precipitates the release of doxorubicin after implantation and light-activation [34]. The elongated residence of CSPM in the tumor tissue may allow the repeatable PDT as we reported in previous study [33].

To evaluate the residual CSPM in tumor, we performed intratumoral injection of CSPM into the CT-26 bearing BALB/c mouse as a model treatment, and confirmed localization and swelling of CSPM through histological observation of the tumor tissue (SI Fig. S7).

3.5. NIR responsive ROS generation of CSPM-PheoA-DFCR microgel

After the conjugation of DFCR to CSPM-PheoA microgel, we evaluated singlet oxygen generation and photo-triggered drug release properties. To examine singlet oxygen generation induced by the activated photosensitizer PheoA in CSPM-PheoA microgel, samples were irradiated using a NIR laser in the presence of the fluorescent probe DMA (9, 10-dimethylanthracene). DMA is a well-known singlet oxygen-sensitive blue fluorescence dye that can be used as a singlet oxygen

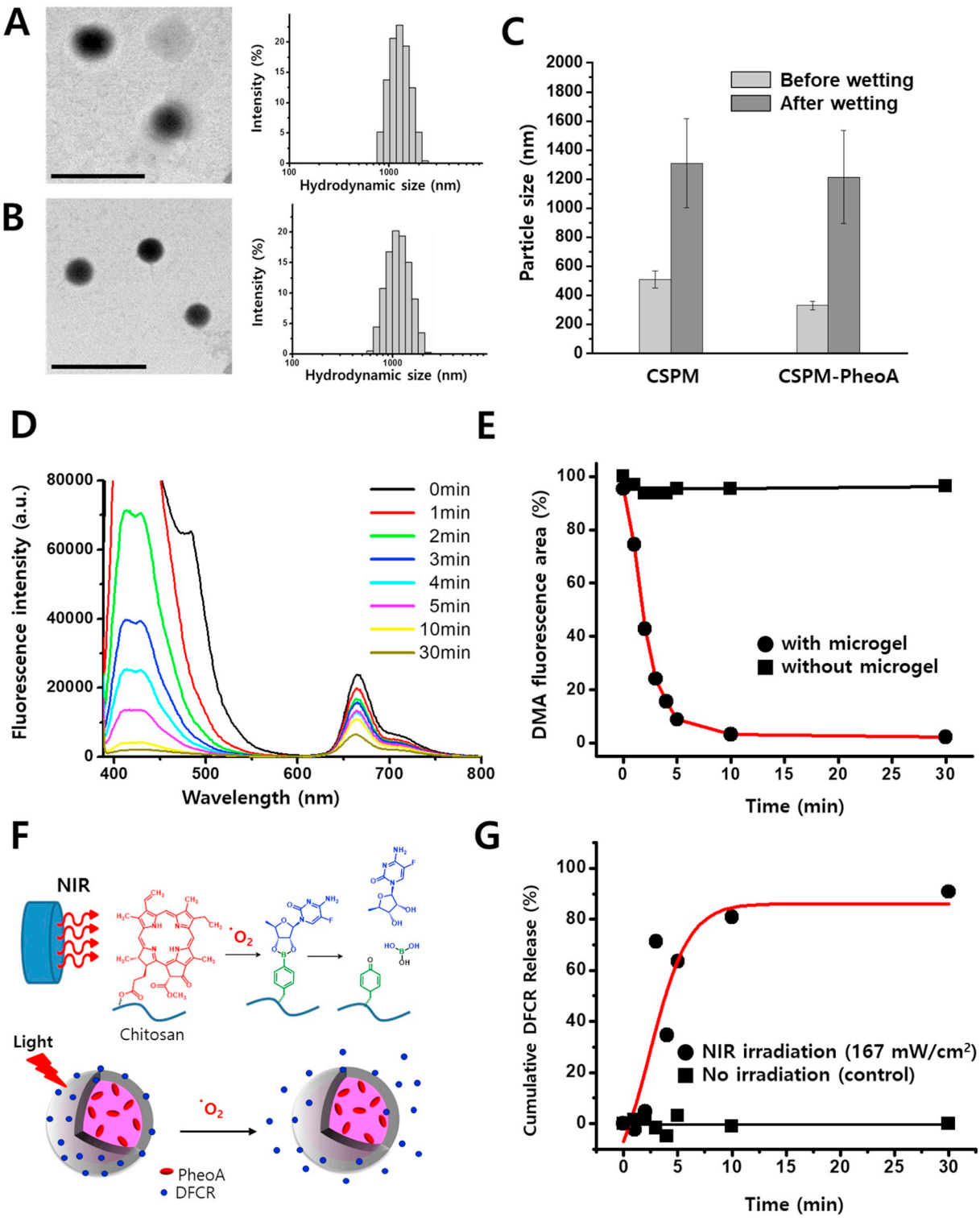

Fig. 3. Combination characteristics (Water swelling, ROS generation and DRCR release) of CSPM-PheoA microgels. (A, B and C) Water swelling properties of CSPM-PheoA microgels. The average particle size of CSPM microgels (A) and CSPM-PheoA microgels (B) in hydrated and dried state. Hydrodynamic sizes of CSPM microgels and CSPM-PheoA microgels in DW were 1309 ± 306 and 1214 ± 320 nm, respectively, and their TEM sizes estimated under dry state were 511 ± 59 and 332 ± 30 nm, respectively (Scale bar = 1 μm). (C) After subtumoral injection, microgels are supposed to absorb the boy fluids, swell and localize at the tumoral lesion. (D and E) NIR triggered ROS generation of CSPM-PheoA microgels. (D) The fluorescence spectra of 9, 10-dimethylanthracene (DMA, 100 μM) after photo-decomposition by ROS generation. CSPM-PheoA microgels (4.5 mg/mL) were co-incubated with DMA and irradiated with 670 nm laser (power; 167 mW/cm^2, time; 1, 2, 3, 4, 5, 10, and 30 min). (E) Fluorescence spectra area of DMA (380–600 nm range) with/without microgel. The decreased fluorescence intensity and spectral area suggested generation of ROS from CSPM-PheoA microgels. (F and G) ROS-triggered release of DFCR. (F) Mechanism of boronic ester cleavage by hydrogen peroxide derived from activated photosensitizer PheoA. (G) ROS-triggered drug release from CSPM-PheoA-DFCR microgels analyzed by HPLC. The microgel samples (5 mg/mL) in DMSO were exposed to NIR laser (λ = 670 nm, 167 mW/cm^2, irradiation time = 1, 2, 3, 4, 5, 10, and 30 min, respectively). And the released DFCR in sample sloution was measured by HPLC [injection volume = 10 μL; elution buffer = DW/Methanol (8:2, *v*/v), absorbance at 220 nm, retention time = 4.15 min].

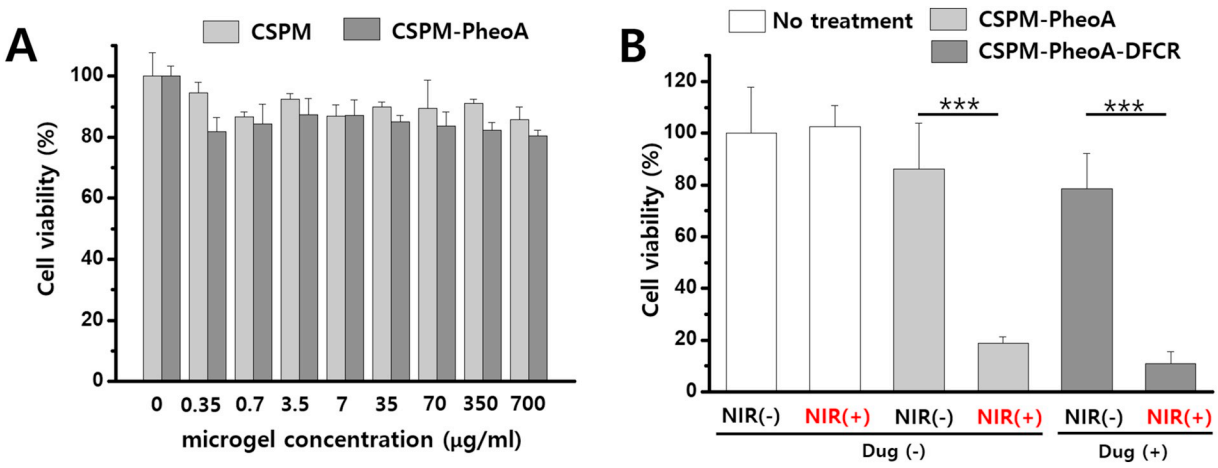

Fig. 4. Concentration-dependent cellular toxicity of CSPM and CSPM-PheoA microgel (A) and NIR-induced PDT effect (B). (A) PANC-1 cells were treated with microgel and cell viability test (WST-1 assay) was performed after three days. To evaluate the PDT effect of the photosensitizer PheoA in microgel, the cells in DMEM medium were treated with CSPM-PheoA and CSPM-PheoA-DFCR in DMSO (final concentration 65 μg/mL, 5% DMSO in medium) and exposed to NIR laser [λ = 671 nm, 100 J/cm^2, NIR(+) or NIR(−)]. After 2 h of incubation, cell viability was measured using a UV–Vis spectrometer (tested individual sample set, n = 5., ***P < .001 by student t-test).

detector by fluorescence quenching by endoperoxide anthracene formation, as previously described [30].

To evaluate singlet oxygen generation by the synthesized CSPM-PheoA-DFCR complex, DMA (final concentration 100 μM) was added to the samples and DMA fluorescence intensities were measured using fluorospectrometer after samples irradiation with the NIR laser (671 nm, 167 mW/cm^2) for 1 to 30 min (Fig. 3D). The fluorescence intensities of DMA (380–600 nm) and PheoA (600–800 nm) in CSPM-PheoA-DFCR microgel were found to decrease steadily on increasing exposure time. As a control experiment, DMA solution without microgel was also exposed to NIR for the same times, but no change in fluorescence intensity was observed (data not shown). A plot of the fluorescence quenching profile of DMA versus NIR irradiation time (Fig. 3E). In Fig. 3E, the exposure of the microgel to NIR with constant light intensity gradually increased the singlet oxygen generation depending on time, and most of generated singlet oxygen started to saturate after 10 min. In the control without microgel, there was no fluorescence quenching of DMA under NIR irradiation and it is indicating that the singlet oxygen was generated by the PheoA in the microgels and the singlet oxygen generating efficiency of CSPM-PheoA-DFCR was greatest at energies > 100 J/cm^2.

3.6. ROS triggered DFCR release from CSPM-PheoA-DFCR microgel

To confer an ROS-triggered drug release property to the microgel, PBA (phenylboronic acid) was used to link the microgel and DFCR, as previously described [35–37]. In the present study, we synthesized a complex by boronic ester linkage between PBA and DFCR, and conjugated the complex formed with CSPM-PheoA by reacting the amine (–NH_2) group of D-glucosamine in chitosan with the hydroxyl (-OH) moiety of the 4-hydroxymethyl group in PBA-DFCR complex to form ester linkages (Fig. 1C). CSPM-PheoA-DFCR was purified by dialysis in the presence of DMSO, and then used for the photo-triggered drug release experiment (Fig. 3E). HPLC was used to obtain plots of DFCR release versus NIR irradiation time (Fig. 3G). As shown in Fig. 3G, NIR initiated DFCR release from CSPM-PheoA-DFCR microgel and released DFCR were reached saturation at 10 min. Non-irradiated control samples did not show any evidence of DFCR release. These results suggest that the DFCR release of CSPM-PheoA-DFCR under NIR irradiation occurs simultaneously with the singlet oxygen generation in Fig. 3E. Moreover, we further.

To evaluate the effect of generated ROS and H_2O_2 from microgel under NIR irradiation, we further performed the cellular imaging study in the presence of DCFDA (2′,7′-dichlorofluorescine diacetate). DCFDA is a fluorescent indicator which is showing strong fluorescent in the oxidized state [38]. As shown in SI Fig. S8, CT-26 cell, itself, and CSPM-PheoA-DFCR treated cell without NIR showed no cellular toxicity and no fluorescence of DCFDA. But in the case of CSPM-PheoA-DFCR treated cells with NIR or H_2O_2 exposure, cell populations were reduced and DFCR fluorescence also increased into the cell. This result indicates that cellular toxicity was clearly induced by ROS or H_2O_2 the under NIR irradiation.

3.7. ROS and DFCR combined cytotoxic effect of CSPM-PheoA-DFCR microgel

To evaluate the potential therapeutic effects of CSPM-PheoA-DFCR, we investigated its cellular toxicity using PANC-1 cancer cells. As shown in Fig. 4A, when the cells were incubated with CSPM or CSPM-PheoA microgels in the concentration range 0.35–700 μg/mL (final concentration) for three days, no significant toxicity (≥80% cell viability) was observed. Similarly, CSPM-PheoA-DFCR had no observed toxic effect (data not shown). To investigate the cellular toxicities of microgels exposed to NIR, PANC-1 cells were treated with CSPM-PheoA or CSPM-PheoA-DFCR and then irradiated. As shown in Fig. 4B, in the absence of microgel, control cells were not affected by NIR (100 J/cm^2), whereas after exposure to NIR, cells treated with CSPM-PheoA or CSPM-PheoA-DFCR showed significant reductions in viability (< 20%). According to the results, obtained the cytotoxic effect of CSPM-PheoA-DFCR was slightly greater than that of CSPM-PheoA. Our CSPM microgel is very large in size (~1 um in water) and it is expected to have low efficiency of cellular uptake and ROS diffusion. However, interestingly, the PDT effect of CSPM-PheoA and CSPM-PheoA-DFCR showed > 80% cytotoxicity. This result implies that the ROS generated by PheoA of inside microgel clearly affected the cell even though the limitations such as short half-life and short diffusion distance. This result also suggests that amine rich chitosan shell of microgel is positively charged and bind negatively charged cellular membrane more efficiently, resulting in increased intracellular ROS diffusion and toxicity.

We also performed a cellular imaging study on microgel-treated PANC-1 cells (Fig. 5). After growing cells to ~80% confluency, microgels were added, and cells were incubated for 2 h. They were then irradiated with NIR and incubated for another 2 h. To determine viability, cells were further treated with the live/dead cell staining dyes (NucBlue® Live, NucGreen® Dead, molecular probes) and Fluorescence images were obtained using a confocal microscope (FV1000, Olympus,

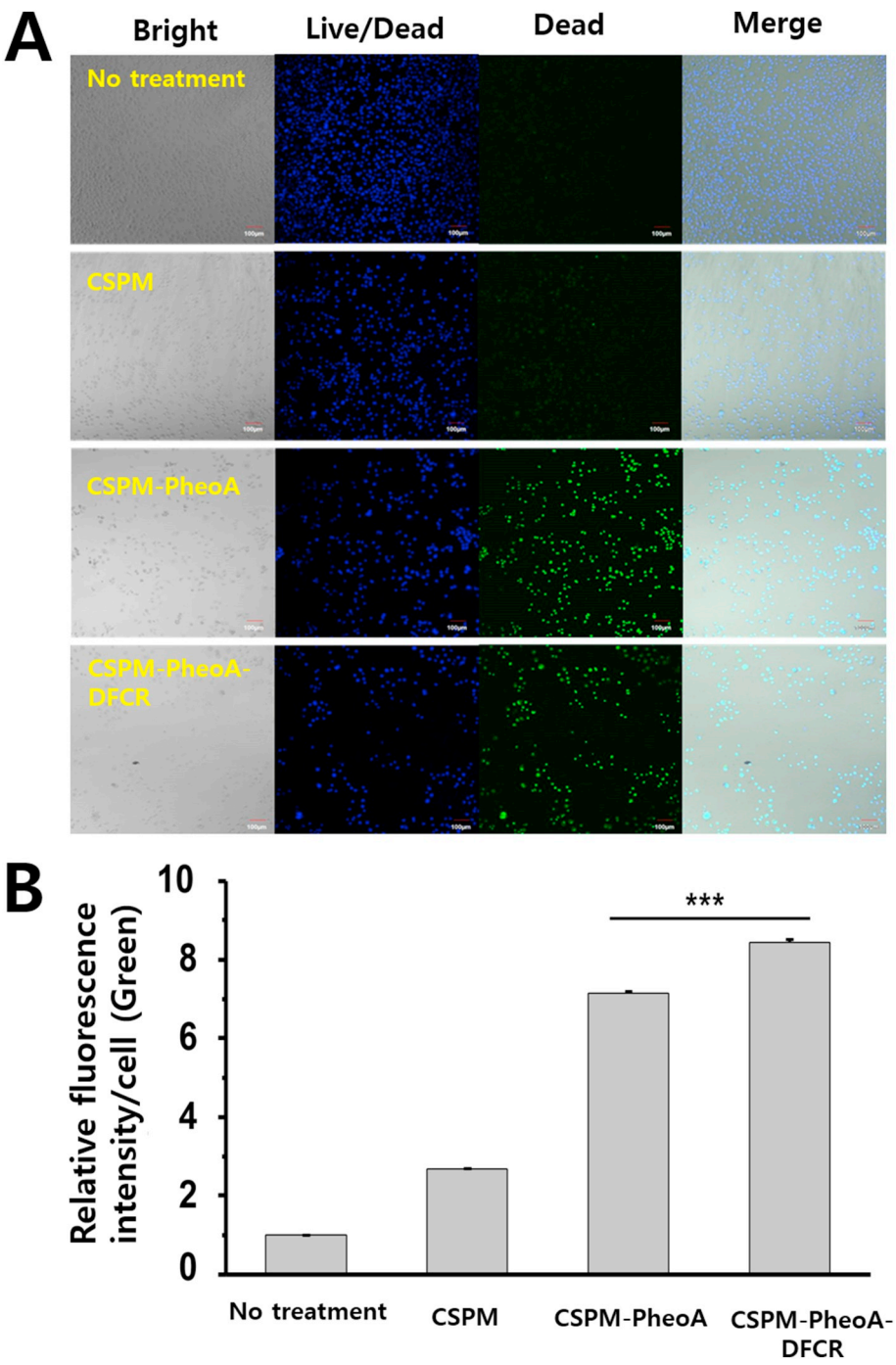

Fig. 5. Microscopic images of NIR-exposed PANC-1 cells after different microgel treatments (A) histogram showing non-viable cell populations after various treatments (B). (A) CSPM, CSPM-PheoA, and CSPM-PheoA-DFCR microgels (0.23 mg/mL) were incubated with PANC-1 cells for 2 h, and cells were then irradiated using a NIR laser (167 mW/cm^2) for 10 min. Cell images were obtained using a confocal microscope (FV1000, Olympus, Japan); the scale bar represents 100 μm. (B) Relative fluorescence intensities/cell as determined using ImageJ software; 1 (No treatment, # of cells: 1620), 2.68 (CSPM, # of cells: 667), 7.14 (CSPM-PheoA, # of cells: 384), and 8.43 (CSPM-PheoA-DFCR, # of cells: 252). Five individual samples were tested, ***P < .001 by the students' t-test.

Japan). Control (no treatment) and CSPM microgel-treated PANC-1 cells showed weak green nuclear fluorescence after NIR irradiation, whereas CSPM-PheoA and CSPM-PheoA-DFCR treated cells showed strong green fluorescence and fewer cells in regions of interest (512 × 512 pixels) due to the detachment of dead cells from the bottoms of glass culture plates. Fluorescence image analysis using ImageJ (NIH, Bethesda, MD) showed the intensity of green fluorescence (dead cells) for CSPM-PheoA-5′DFCR was statistically greater than that of CSPM-PheoA (Fig. 5B). These results were consistent with those of the cellular toxicity study (Fig. 4).

3.8. Inhibition of colon cancer growing through combination cancer therapy

To evaluate the therapeutic efficacy of CSPM-PheoA-DFCR microgel in vivo, we used CT-26 (a murine colon cancer cell-line) bearing BALB/c mice. After allowing tumors to grow to ~100 mm^3, same amounts of CSPM, CSPM-PheoA, or CSPM-PheoA-DFCR microgels (10 mg/kg) were directly injected into tumors. During the study, tumor sizes and body weights of microgel injected mouse were monitored for two weeks. CSPM-PheoA and CSPM-PheoA-DFCR plus NIR exposure effectively suppressed tumor growth (Fig. 6A), though no intergroup differences were observed between body weights (Fig. 6B). Especially, NIR irradiated tumor with CSPM-PheoA-DFCR showed more effective tumor suppression effect compared with that of CSPM-PheoA after 2 weeks (SI Fig. S9).

In addition, hematoxylin and eosin (H&E) and terminal deoxynucleotidyl transferase-mediated dUTP-biotin nick end labeling (TUNEL) staining of tumor slices was performed (Fig. 6C and D). It was

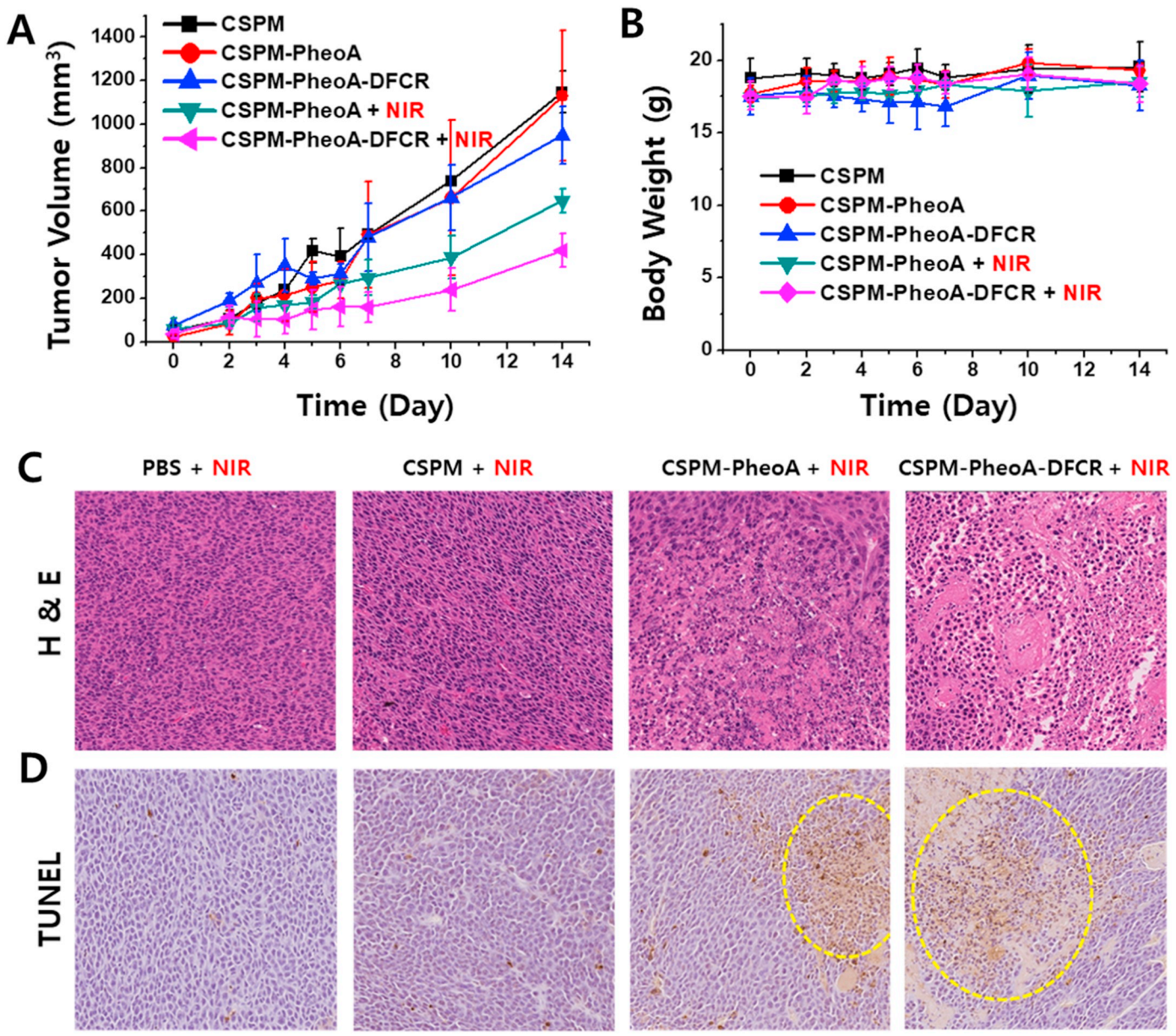

Fig. 6. In vivo CSPM-PheoA-DFCR plus NIR treatment. (A) Growth curves of CT-26 tumors in BALB/c mice after treatments; (L): NIR laser irradiation (λ = 671 nm, 100 J/cm^2). Microgels were directly injected into tumors at 10 mg/kg of body weight. (B) changes in body weights during treatment. (C) H&E and TUNEL stained tumor slices obtained after 14 days of treatment.

found CSPM-PheoA or CSPM-PheoA-DFCR plus NIR produced higher levels of cancer cell apoptosis and necrosis compared to other groups, PBS plus or CSPM plus NIR.

Generally, synergistic therapeutic effect of combination treatment can be acquired from multiple inhibition of cancer molecular pathways or oncogenes. In this study, we investigated combination effect of two functional drugs (DFCR for inhibition of DNA synthesis and PheoA for ROS induced cancer apoptosis) using the microgel delivery system with NIR-triggered release mechanism. As mentioned in above, Ortner et al. clearly showed synergistic therapeutic effect of PDT. They reported combination of PDT with conventional treatment dramatically elongated survival of bile duct cancer patients (493 days of median survival in combination therapy to median 98 days in conventional treatment; $P < .0001$) [10]. And CSPM-PheoA-DFCR with NIR exposure showed most strong cancer growth inhibition efficacy at in vivo and in vitro studies. This therapeutic efficacy may be partly come from simple additive effect or partly from synergic therapeutic effect. In any case, we demonstrated clearly the therapeutic function of the combination of PDT and chemotherapy in this study.

4. Conclusion

In summary, we successfully synthesized a CSPM-PheoA-DFCR microgel with photo-triggered drug release properties for combination cancer therapy. Specifically, CSPM-PheoA-DFCR microgel has core-shell structure, that is, ROS-generation PheoA in poly-HEMA core system and DFCR-releasing chitosan shell. To confirm singlet oxygen generation, CSPM-PheoA-DFCR was exposed to NIR irradiation and then examined using a DMA fluorescence probe technique, which demonstrated ROS generation increased with NIR exposure, and that this was accompanied ROS-induced DFCR release. In addition, CSPM-PheoA-DFCR were investigated in vitro using a pancreatic cancer cell model, in which they showed more effective cellular toxicity due to the DFCR drug release from microgel by NIR irradiation. Furthermore, the

combination effects of CSPM-PheoA-DFCR plus NIR combination therapy were clearly observed in vivo in a colon cancer murine model. Our results suggest that the CSPM-PheoA-DFCR microgel with PDT and ROS-triggerable chemotherapeutic effect can be utilized as a potential material for more effective anti-cancer therapy.

Acknowledgements

This research was supported by the Basic Science Research Program and the Korea Research Fellowship Program through the National Research Foundation of Korea (NRF) (grant no. 2017R1A2A2A07001272, 2017R1D1A1B03035654, and 2018R1A6A1A03025523).

Conflicts of interest

The authors declare that they have no conflicts of interest to declare.

Appendix A. Supplementary data

The supporting Information is available free of charge on the ACS Publications website at DOI: FT-IR spectrum, UV–Vis spectrum, ^{1}H NMR, TEM, photo images were included. Supplementary data to this article can be found online at https://doi.org/10.1016/j.jconrel.2019.05.016.

References

[1] C. Sawyers, Targeted cancer therapy, Nature 432 (2004) 294–297.
[2] K. Imai, A. Takaoka, Comparing antibody and small-molecule therapies for cancer, Nat. Rev. Cancer 6 (2006) 714–727.
[3] S. Hoelder, P.A. Clarke, P. Workman, Discovery of small molecule cancer drugs: successes, challenges and opportunities, Mol. Oncol. 6 (2012) 155–176.
[4] D.B. Longley, P.G. Johnston, Molecular mechanisms of drug resistance, J. Pathol. 205 (2005) 275–292.
[5] C. Swanton, Intratumor heterogeneity: evolution through space and time, Cancer Res. 72 (2012) 4875–4882.
[6] C. Holohan, S. Van Schaeybroeck, D.B. Longley, P.G. Johnston, Cancer drug resistance: an evolving paradigm, Nat. Rev. Cancer 13 (2013) 714–726.
[7] C.M. Peterson, J.M. Lu, Y. Sun, C.A. Peterson, J.G. Shiah, R.C. Straight, J. Kopecek, Combination chemotherapy and photodynamic therapy with N-(2-hydroxypropyl) methacrylamide copolymer-bound anticancer drugs inhibit human ovarian carcinoma heterotransplanted in nude mice, Cancer Res. 56 (1996) 3980–3985.
[8] R. Baskaran, J. Lee, S.G. Yang, Clinical development of photodynamic agents and therapeutic applications, Biomater Res 22 (2018) 25.
[9] H. Witzigmann, F. Berr, U. Ringel, K. Caca, D. Uhlmann, K. Schoppmeyer, A. Tannapfel, C. Wittekind, J. Mossner, J. Hauss, M. Wiedmann, Surgical and palliative management and outcome in 184 patients with hilar cholangiocarcinoma - palliative photodynamic therapy plus stenting is comparable to R1/R2 resection, Ann. Surg. 244 (2006) 230–239.
[10] M.E.J. Ortner, K. Caca, F. Berr, J. Liebetruth, U. Mansmann, D. Huster, W. Voderholzer, G. Schachschal, J. Mossner, H. Lochs, Successful photodynamic therapy for nonresectable cholangiocarcinoma: a randomized prospective study, Gastroenterology 125 (2003) 1355–1363.
[11] P. Thapa, M.J. Li, M. Bio, P. Rajaputra, G. Nkepang, Y.J. Sun, S. Woo, Y. You, Far-red light-Activatable Prodrug of paclitaxel for the combined effects of photodynamic therapy and site-specific paclitaxel chemotherapy, J. Med. Chem. 59 (2016) 3204–3214.
[12] L.H. Liu, W.X. Qiu, L. Bin, C. Zhang, L.F. Sun, S.S. Wan, L. Rong, X.Z. Zhang, A red light Activatable multifunctional Prodrug for image-guided photodynamic therapy and cascaded chemotherapy, Adv. Funct. Mater. 26 (2016) 6257–6269.
[13] Y. Wang, G.Q. Wei, X.B. Zhang, F.N. Xu, X. Xiong, S.B. Zhou, A step-by-step multiple stimuli-responsive Nanoplatform for enhancing combined chemo-photodynamic therapy, Adv. Mater. 29 (2017) 1605357.
[14] R. Wentrup, N. Winkelmann, A. Mitroshkin, M. Prager, W. Voderholzer, G. Schachschal, C. Jurgensen, C. Buning, Photodynamic therapy plus chemotherapy compared with photodynamic therapy alone in Hilar Nonresectable Cholangiocarcinoma, Gut Liver 10 (2016) 470–475.
[15] B.C. Bae, S.G. Yang, S. Jeong, D.H. Lee, K. Na, J.M. Kim, G. Costamagna, R.A. Kozarek, H. Isayama, J. Deviere, D.W. Seo, D. Nageshwar Reddy, Polymeric photosensitizer-embedded self-expanding metal stent for repeatable endoscopic photodynamic therapy of cholangiocarcinoma, Biomaterials 35 (2014) 8487–8495.
[16] J.J. Liu, G.B. Yang, W.W. Zhu, Z.L. Dong, Y. Yang, Y. Chao, Z. Liu, Light-controlled drug release from singlet-oxygen sensitive nanoscale coordination polymers enabling cancer combination therapy, Biomaterials 146 (2017) 40–48.
[17] H.R. Jia, Y.X. Zhu, K.F. Xu, F.G. Wu, Turning toxicants into safe therapeutic drugs: Cytolytic peptide-photosensitizer assemblies for optimized in vivo delivery of Melittin, Adv. Healthc. Mater. 7 (2018) 1800380.
[18] Y.X. Zhu, H.R. Jia, G.Y. Pan, N.W. Ulrich, Z. Chen, F.G. Wu, Development of a light-controlled Nanoplatform for direct nuclear delivery of molecular and Nanoscale materials, J. Am. Chem. Soc. 140 (2018) 4062–4070.
[19] C.S. Xiao, J.X. Ding, L.L. Ma, C.G. Yang, X.L. Zhuang, X.S. Chen, Synthesis of thermal and oxidation dual responsive polymers for reactive oxygen species (ROS)-triggered drug release, Polym. Chem. 6 (2015) 738–747.
[20] K. Kim, C.S. Lee, K. Na, Light-controlled reactive oxygen species (ROS)-producible polymeric micelles with simultaneous drug-release triggering and endo/lysosomal escape, Chem. Commun. 52 (2016) 2839–2842.
[21] S.S. Yu, R.L. Koblin, A.L. Zachman, D.S. Perrien, L.H. Hofmeister, T.D. Giorgio, H.J. Sung, Physiologically relevant oxidative degradation of Oligo(proline) cross-linked polymeric scaffolds, Biomacromolecules 12 (2011) 4357–4366.
[22] Y. Cha, M.J. Han, H.J. Cha, J. Zoldan, A. Burkart, J.H. Jung, Y. Jang, C.H. Kim, H.C. Jeong, B.G. Kim, R. Langer, C.R. Kahn, L. Guarente, K.S. Kim, Metabolic control of primed human pluripotent stem cell fate and function by the miR-200c-SIRT2 axis, Nat. Cell Biol. 19 (2017) 445–456.
[23] M. Alcalá, M. Calderon-Dominguez, E. Bustos, P. Ramos, N. Casals, D. Serra, M. Viana, L. Herrero, Increased inflammation, oxidative stress and mitochondrial respiration in brown adipose tissue from obese mice, Sci. Rep. 7 (2017) 16082.
[24] O.A. Khomich, S.N. Kochetkov, B. Bartosch, A.V. Ivanov, Redox biology of respiratory viral infections, Viruses 10 (2018).
[25] I. Postiglione, A. Chiaviello, G. Palumbo, Enhancing Photodynamyc therapy efficacy by combination therapy: dated, current and oncoming strategies, Cancers 3 (2011) 2597–2629.
[26] K. El-Tahlawy, S.M. Hudson, Graft copolymerization of hydroxyethyl methacrylate onto chitosan, J. Appl. Polym. Sci. 82 (2001) 683–702.
[27] G. Springsteen, B.H. Wang, A detailed examination of boronic acid-diol complexation, Tetrahedron 58 (2002) 5291–5300.
[28] S. Jenjob, M. Ratanajanchai, N. Mahattanadul, S. Soodvilai, P. Sunintaboon, Synthesis of a biocompatible poly(2-hydroxyethyl methacrylate)chitosan Core-Shell hydrogel latex, J. Appl. Polym. Sci. 131 (2014) 40003.
[29] L. Zhao, T.H. Kim, H.W. Kim, S.Y. Kim, Pheophorbide a-conjugated pH-sensitive nanoparticle vectors for highly efficient photodynamic therapy of Cancer, Int. J. Polym. Mater. Polym. Biomater. 64 (2015) 733–744.
[30] S. Martins, J.P.S. Farinha, C. Baleizao, M.N. Berberan-Santos, Controlled release of singlet oxygen using diphenylanthracene functionalized polymer nanoparticles, Chem. Commun. 50 (2014) 3317–3320.
[31] T. Li, L.F. Ma, R.Y. Bao, G.Q. Qi, W. Yang, B.H. Xie, M.B. Yang, A new approach to construct segregated structures in thermoplastic polyolefin elastomers towards improved conductive and mechanical properties, J. Mater. Chem. A 3 (2015) 5482–5490.
[32] N. Vennemann, K. Bökamp, D. Dirk Bröker, Crosslink density of peroxide cured TPV, Macromol. Symp. 245-246 (2006) 641–650.
[33] Y. Danyuo, S. Dozie-Nwachukwu, J.D. Obayemi, C.J. Ani, O.S. Odusanya, Y. Oni, N. Anuku, K. Malatesta, W.O. Soboyejo, Swelling of poly(N-isopropylacrylamide) P(NIPA)-based hydrogels with bacterial-synthesized prodigiosin for localized cancer drug delivery, Mater. Sci. Eng. C-Mater. Biol. Appl. 59 (2016) 19–29.
[34] C.Y. Xing, S.Y. Chen, X. Liang, Q. Liu, M.M. Qu, Q.S. Zou, J.H. Li, H. Tan, L.P. Liu, D.Y. Fan, H. Zhang, Two-dimensional MXene (Ti3C2)-integrated cellulose hydrogels: toward smart three-dimensional network Nanoplatforms exhibiting light-induced swelling and bimodal Photothermal/chemotherapy anticancer activity, ACS Appl. Mater. Interfaces 10 (2018) 27631–27643.
[35] H.G. Kuivila, A.G. Armour, Electrophilic displacement reactions. IX. Effects of substituents on rates of reactions between hydrogen peroxide and Benzeneboronic acid, Journal of American Chemical Society 79 (1957) 5659–5662.
[36] Y.Y. Kuang, K. Baakrishnan, V. Gandhi, X.H. Peng, Hydrogen peroxide inducible DNA cross-linking agents: targeted anticancer Prodrugs, J. Am. Chem. Soc. 133 (2011) 19278–19281.
[37] R. Kumar, J. Han, H.J. Lim, W.X. Ren, J.Y. Lim, J.H. Kim, J.S. Kim, Mitochondrial induced and self-monitored intrinsic apoptosis by antitumor Theranostic Prodrug: in vivo imaging and precise Cancer treatment, J. Am. Chem. Soc. 136 (2014) 17836–17843.
[38] X. Wang, M.G. Roper, Measurement of DCF fluorescence as a measure of reactive oxygen species in murine islets of Langerhans, Anal. Methods 6 (2014) 3019–3024.